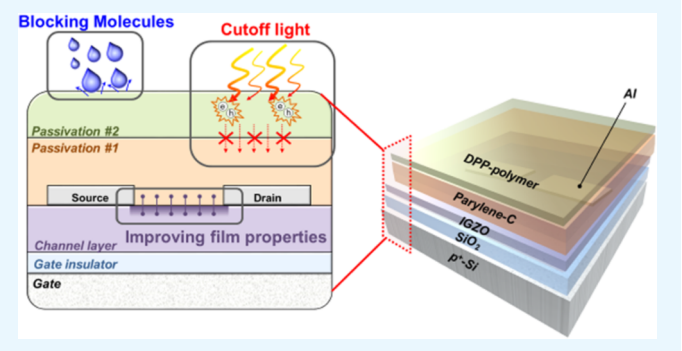


# Multifunctional, Room-Temperature Processable, Heterogeneous Organic Passivation Layer for Oxide Semiconductor Thin-Film **Transistors**

Young Jun Tak, Scott Tom Keene, Byung Ha Kang, Won-Gi Kim, Si Joon Kim, Alberto Salleo,\*,\$ and Hyun Jae Kim\*,‡

Supporting Information

ABSTRACT: In recent decades, oxide thin-film transistors (TFTs) have attracted a great deal of attention as a promising technology in terms of next-generation electronics due to their outstanding electrical performance. However, achieving robust electrical characteristics under various environments is a crucial challenge for successful realization of oxide-based electronic applications. To resolve the limitation, we propose a highly flexible and reliable heterogeneous organic passivation layer composed of stacked parylene-C and diketopyrrolopyrrole-polymer films for improving stability of oxide TFTs under various environments and mechanical stress. The presented multifunctional heterogeneous organic (MHO) passivation



leads to high-performance oxide TFTs by: (1) improving their electrical characteristics, (2) protecting them from external reactive molecules, and (3) blocking light exposure to the oxide layer. As a result, oxide TFTs with MHO passivation exhibit outstanding stability in ambient air as well as under light illumination: the threshold voltage shift of the device is almost 0 V under severe negative bias illumination stress condition (white light of 5700 lx, gate voltage of -20 V, and drain voltage of 10.1 V for 20 000 s). Furthermore, since the MHO passivation layer exhibits high mechanical stability at a bending radius of ≤5 mm and can be deposited at room temperature, this technique is expected to be useful in the fabrication of flexible/wearable devices.

KEYWORDS: oxide semiconductor, thin-film transistor, passivation layer, DDP-polymer, parylene-C

# 1. INTRODUCTION

For several decades, information displays have been fabricated on flat glass panels. However, in recent days, the demand for lighter, unbreakable, and flexible displays is increasing rapidly. To satisfy these desires of consumers, various plastic substrates for electronic devices (polyimide, poly(ethylene terephthalate), and poly(ethylene naphthalate)) have been developed, and display backplanes have been fabricated on such substrates. Therefore, fabricating thin-film transistors (TFTs), a basic driving unit for display backplanes, on plastic substrates is one of the most challenging and important tasks for realizing flexible devices. To realize the technology, materials of electrodes, gate dielectric layers, and channel layers of flexible TFTs have been extensively studied. Among them, numerous types of channel materials are mainly investigated since the channel layer, serving as a semiconducting carrier-transport layer, crucially affects electrical characteristics of the device, such as field-effect mobility, on/off ratio, threshold voltage  $(V_{\rm TH})$ , and so on.

Among the various materials for TFT channels, oxide semiconductors, especially indium-gallium-zinc-oxide (IGZO), have been regarded as promising candidates for use in nextgeneration displays due to their relatively high field-effect mobility ( $\sim 10 \text{ cm}^2/(\text{V s})$ ) even when fabricated below 200 °C, high uniformity over large areas, high transparency (~90%) in the visible region, and low off-current (in the pA range). 1-5 Such performance metrics have led to their remarkable development, to the point where many commercial display products are currently manufactured using oxide TFTs.<sup>6,7</sup>

Although oxide TFTs show exceptional electrical performance, they are unstable in ambient environments. Since the oxide semiconductor exhibits ionic bonding configuration, which has relatively lower bonding energy compared to other bonding configurations (covalent and van der Waals bonding),

Received: September 18, 2019 Accepted: December 18, 2019 Published: December 18, 2019

<sup>&</sup>lt;sup>†</sup>School of Electrical and Electronic Engineering, Yonsei University, 50 Yonsei-ro, Seodaemun-gu, Seoul 03722, Republic of Korea <sup>‡</sup>Department of Electrical and Electronics Engineering, Kangwon National University, 1 Gangwondaehakgil, Chuncheon-si, Gangwon-do 24341, Republic of Korea

<sup>&</sup>lt;sup>§</sup>Materials Science and Engineering, Stanford University, Stanford, California 94305, United States

there is a high possibility of possessing more uncoordinated surface defects such as metal ions and oxygen vacancies. These uncoordinated surface defects tend to interact with adsorbed molecules from ambient gas, a kind of redox process, and lead to variation in the number of effective carriers. Furthermore, the ionic bonds are unstable under light illumination; uncoordinated oxygen species in oxide films can be readily ionized given that their bonding energies (2.0–2.3 eV) are lower than those of covalent bonds (e.g., 3.5 eV for Si–Si).  $^{10-12}$  Thus, the electrical characteristics of oxide TFTs working in ambient environments may degrade, typically shifting the  $V_{\rm TH}$ , increasing the subthreshold swing (S.S) and off-current, and reducing field-effect mobility.  $^{13-15}$ 

One facile strategy to overcome these stability issues is to passivate the surface of the oxide semiconductor. This passivation (PVX) layer can protect oxide semiconductors from penetrating water and oxygen molecules from the external environment to prevent unwanted redox reactions. Furthermore, since such passivation engineering is a more facile process compared to structural engineering and various post-treatments of oxide TFTs, it can achieve a higher manufacturing cost competitiveness.

Meanwhile, recently, beyond the intrinsic concept of the passivation layer, some research groups have reported that passivation layers cannot only improve stability against the external environment (intrinsic blocking properties) but also enhance the electrical characteristics of oxide TFTs by destroying uncoordinated oxygen species via chemical reactions with the channel layer. 19,20 This enhanced electrical performance results from the migration of oxidizing atoms from the passivation layer to the oxide-passivation layer interface, which can increase the number of metal-oxide bonds and decrease the number of oxygen vacancies in the oxide channel layer. In addition, elimination of uncoordinated oxygen species improves oxide TFT stability under light illumination. A reduced number of uncoordinated oxygen species is associated with less generation of (unwanted) excessive carriers by photon energy-induced ionization. Another study reported that inserting an interfacial organic layer between the oxide channel and copper (Cu) source/drain electrodes improved the electrical characteristics of the TFT as well as blocked the migration of Cu ions while passivating the oxide surface.<sup>21</sup> Further, this interfacial layer could be fabricated at low temperature, allowing the use of temperature-sensitive flexible substrates (e.g., polyimide, poly-(ethylene terephthalate), etc.) favored in flexible/wearable applications. Like those reports, many studies have extensively investigated the placing of many functions into the passivation layer for improving electrical characteristics and stability of oxide TFTs.

In this study, we suggest multifunctional heterogeneous organic (MHO) passivation for oxide TFTs, which can provide a new approach for designing of the passivation layer consisting of layers with different functions. This novel structured passivation layer will provide both improved electrical characteristics and stability of oxide TFTs under various environments. Furthermore, since the MHO layer can be fabricated at room temperature without any additional thermal treatment and exhibits high mechanical stability, it is expected to be highly suitable for flexible/wearable applications.

# 2. EXPERIMENTAL SECTION

- **2.1. Synthesis of Diketopyrrolopyrrole (DPP)-Polymer.** The diketopyrrolopyrrole (DPP) polymer used in this study is composed of two kinds of DPP-based semiconducting polymers: poly{3-([2,2':5',2''-terthiophen]-5-yl)-2,5-bis(2-octyldodecyl)-2,5-dihydropyrrolo[3,4-c]pyrrole-1,4-dione-6,5''-diyl} [P(DPP2ODT2-T); TE223] and poly{3-([2,2':5',2''-terthiophen]-5-yl)-2,5-bis(6-dodecyloctadecyl)-2,5-dihydropyrrolo[3,4-c]pyrrole-1,4-dione-6,5''-diyl} [P(DPP6DOT2-T); TE239], which were synthesized by palladium-catalyzed Stille coupling polycondensation as previously described in the literature. <sup>22,23</sup> The number average molecular weight ( $M_n$ ) and dispersity ( $D = M_w/M_n$ ) of the copolymers were analyzed by high-temperature gel permeation chromatography (PL-GPC 220; Polymer Laboratories) at 150 °C using 1,2,4-trichlorobenzene. The obtained molecular weights and dispersities were  $M_n = 16.8$  kg/mol and D = 2.3 for P(DPP2ODT2-T) and  $M_n = 19.4$  kg/mol and D = 2.5 for P(DPP6DOT2-T).
- 2.2. Fabrication of IGZO TFTs. To fabricate IGZO TFTs, we prepared a heavily doped p-type Si wafer ( $p^+\text{-Si}$ ) with a thermally grown SiO2 coating, which acts as the gate electrode and the gate insulator, respectively. This substrate was cleaned by immersing acetone and methanol for 10 min in an ultrasonic bath in sequence. After cleaning, IGZO films were deposited on the substrate using a radio frequency (RF) sputter system. The IGZO target is composed of In2O3:Ga2O3:ZnO at 1:1:1 mol %. The conditions of the RF sputter system are RF power, working pressure, and oxygen pressure set to 150 W, 5 mTorr, and 0 Torr, respectively. Following deposition of IGZO films, they were annealed at 300 °C in air for 1 h to exhibit semiconducting properties. Finally, a 200 nm-thick Al source and drain electrodes were deposited with a shadow mask using a thermal evaporator. The length and width of the channel layer were 150 and 1000  $\mu$ m, respectively. Passivation layers of SiO<sub>2</sub> and HfO<sub>x</sub> were fabricated by sputtering and annealed at 250 °C in air for 1 h. Moreover, to fabricate flexible IGZO TFTs, we used a polyimide substrate with 40 nm-thick SiO<sub>2</sub>/200 nm-thick SiN<sub>x</sub> films and Mo metal. The SiO<sub>2</sub>/SiN<sub>x</sub> films and the Mo served as the gate insulator and gate electrode, respectively. Then, cleaning, channel deposition, annealing, and electrode deposition processes were the same as the aforementioned methods.
- 2.3. Fabrication of the MHO Passivation Layer. To construct the MHO passivation layer, we first deposited a 500 nm-thick film of cross-linked parylene-C using an SPS Labcoater parylene deposition system. The prepared IGZO TFTs were placed under vacuum (ca. 0.1 torr) with 4 mL of silane A174 (3-(trimethoxysilyl)propyl methacrylate) cross-linking agent placed on the sidewalls of the deposition chamber. Then, 1 g of parylene-C dimer (dichloro[2,2]paracyclophane) was heated to 680 °C to form a monomer vapor, which flows into the deposition chamber at 25 °C; this condensed and polymerized on the substrate surface, forming a densely crosslinked conformal coating. Then, we coated a DPP-polymer on the IGZO TFTs with parylene-C films as the second layer using spincoating after it was aged for 24 h at room temperature. The spincoating was proceeded with 3000 rpm for 30 s in air at room temperature. After coating the DPP-polymer, it was dried at room temperature for 5 min in air, forming a 50 nm-thick film.
- **2.4. Electrical, Chemical, and Optical Analyses.** The measurements of transfer characteristics were carried out by sweeping a  $V_{\rm GS}$  from -30 to 30 V with a fixed  $V_{\rm DS}$  of 10.1 V, which makes the devices operate in the saturation regime using a Keithley 2400 semiconductor analyzer. The PBS and NBS were measured by applying constant  $V_{\rm GS}$  of 20 and -20 V, respectively, with a  $V_{\rm DS}$  of 10.1 V for 3600 s. The NBIS was measured by applying a constant  $V_{\rm GS}$  of -20 V with  $V_{\rm DS}$  of 10.1 V under light illumination (white light emitting diode (LED) with 5700 lx) for  $20\,000$  s. The change in drain current was measured at a  $V_{\rm GS}$  of -1 V and  $V_{\rm DS}$  of 10.1 V under white LED with 5700 lx and red, green, and blue laser illuminations as a function of power intensity. UV—visible spectroscopy was used to investigate the absorption properties of each film, and scanning electron microscopy (SEM) was used to determine each film's morphology. Atomic force

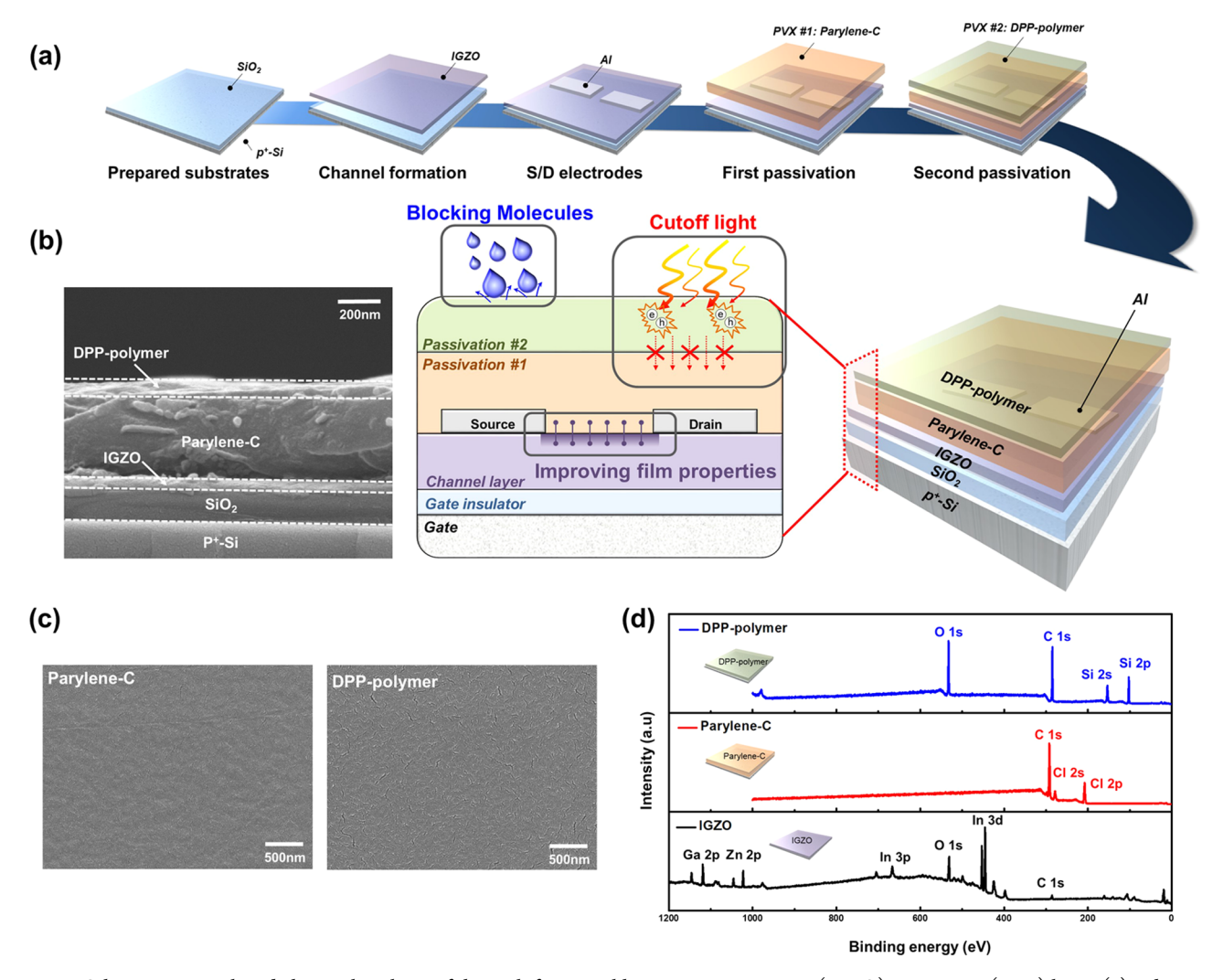


**Figure 1.** Schematic, optical, and chemical analyses of the multifunctional heterogeneous organic (MHO) passivation (PVX) layer. (a) Fabrication process of IGZO TFTs with MHO passivation. (b) Cross-sectional SEM image of IGZO TFTs with MHO passivation and illustration of expected multifunctional effects. (c) Surface SEM image of parylene-C and DPP-polymer films. (d) XPS spectrum of DPP-polymer, parylene-C, and IGZO films.

microscopy (AFM) and contact angle analyzer were used to confirm surface morphologies and properties, respectively. X-ray photoelectron spectroscopy (XPS) was performed to identify chemical compositions and valence band states. In detail, the sputtering power (X-ray beam power) and time for removing the films were 500 eV with 5 min for the DPP-polymer film, 2 keV with 8 min and 5 keV with 22 min for the parylene-C film, and 2 keV with 20 min for the IGZO film, sequentially.

# 3. RESULTS AND DISCUSSION

The MHO passivation consists of two thin films, parylene-C and diketopyrrolepyrrole (DPP) polymer, which are deposited on the back-surface of IGZO TFTs at room temperature using evaporation and spin-coating, respectively (Figure 1a). The materials of MHO passivation layers were chosen to provide the following functionalities: (1) improving the electrical characteristics of IGZO TFTs by eliminating uncoordinated oxygen species from IGZO thin films, (2) passivation against external reactive molecules in atmosphere, and (3) blocking light exposure to the IGZO films. We will discuss later the role of each layer in the MHO-passivated IGZO TFTs. Figure 1b shows a cross-sectional SEM image of IGZO films with MHO passivation layers, showing thicknesses of 40, 500, and 50 nm

for IGZO, parylene-C, and DPP-polymer, respectively. Furthermore, from the surface SEM image of parylene-C and DPP-polymer films (Figure 1c), we observed that each film uniformly covered on the surface of the underlying films. The chemical structures of used parylene-C and DPP-polymer are shown in Figure S1, and the qualitative chemical compositions of IGZO, parylene-C, and DPP-polymer films (as confirmed by XPS analysis) are shown in Figure 1d.

The electrical characteristics and stability of IGZO TFTs with and without passivation layers are presented in Figure 2. From the transfer curves, we observed that IGZO TFTs with parylene-C and MHO passivation exhibited improved electrical characteristics compared to unpassivated IGZO TFTs (Figure 2a-c). Specifically, the passivated IGZO films have lower off-current and higher on-current without any change in the  $V_{\rm TH}$ . We attributed the improved electrical performance to eliminating adsorption of moisture and oxygen onto the back-surface of IGZO, preventing undesirable chemical reactions, which cause increased leakage current by creating charge screening in IGZO films. <sup>24</sup> Furthermore, from the summarized results of the electrical characteristics (Figure 2d) of IGZO TFTs without and with passivation (parylene-C

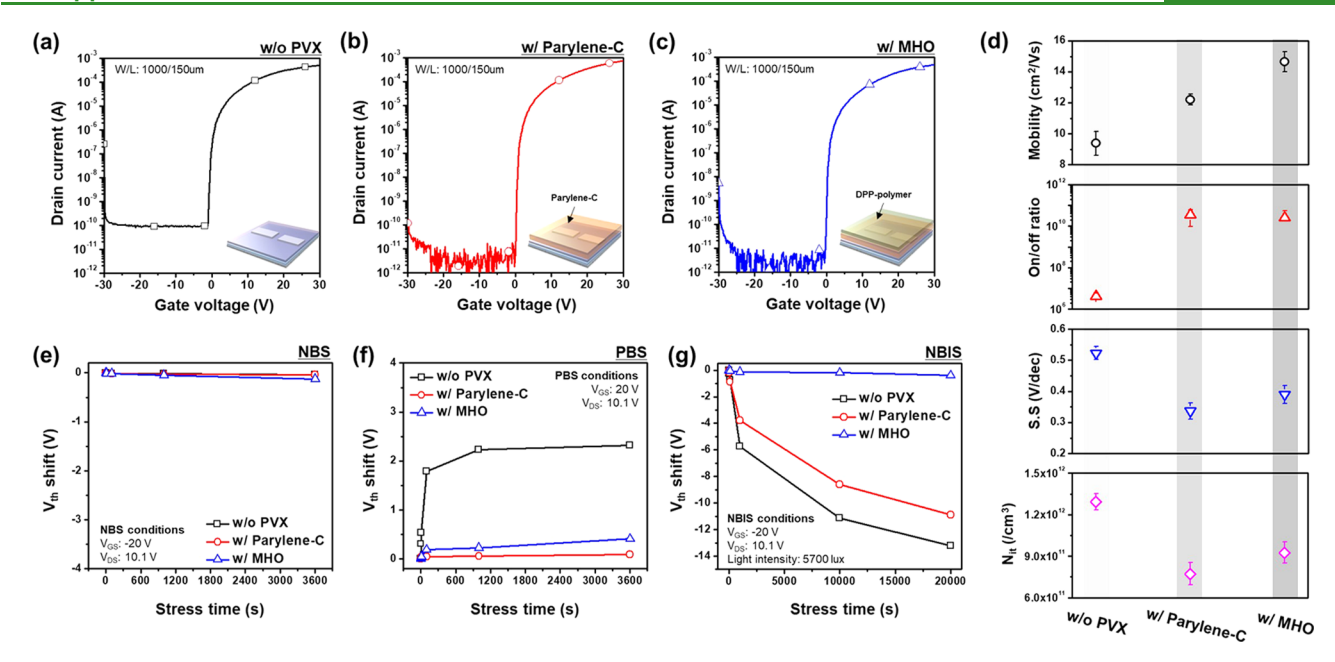


Figure 2. Electrical characteristics and stability of MHO-passivated IGZO TFTs. Transfer characteristics of IGZO TFTs (a) without passivation (PVX) and with (b) parylene-C and (c) MHO passivation. (d) Statistical electrical parameters including mobility, on/off ratio, S.S, and  $N_{it}$  of IGZO TFTs without passivation and with parylene-C and MHO passivation. Threshold voltage shift under (e) NBS, (f) PBS, and (g) NBIS of IGZO TFTs without passivation and with parylene-C and MHO passivation.

and MHO), we observed that the parylene-C modified the chemistry of the IGZO/parylene-C interface.

To explore the stability of IGZO TFTs under voltage bias and light illumination in air, we performed negative bias stress (NBS), positive bias stress (PBS), and negative bias illumination stress (NBIS) tests (Figure 2e-g). In general, bias instabilities under NBS and PBS for IGZO TFTs are caused by either charge trapping at the interface between the gate insulator and the channel layer or charge coupling modulation due to potential energy of adsorbed molecules. 25,2 However, we did not expect to find variations in charge trapping at the interface because all IGZO TFTs in this work have the same interfacial characteristics between gate insulator and channel layers. Therefore, only charge coupling modulation changes would be responsible for the difference in bias stress properties between passivated and unpassivated IGZO TFTs. We found that the  $V_{\rm TH}$  shift was negligible under the NBS test for all IGZO TFTs (Figure 2e); IGZO TFTs passivated with parylene-C and MHO exhibited significantly improved stability under the PBS test compared to those without passivation layers (Figure 2f). In general, the positive shift of  $V_{\rm TH}$  in IGZO TFTs under PBS is due to a decrease in electron density in the IGZO film because adsorbed oxygen at the back-channel region captures an electron from the conduction band of the IGZO channel.<sup>27</sup> Thus, the improved PBS stability of passivated IGZO TFTs can be attributed to the superior blocking ability of parylene-C and MHO films preventing the adsorption of oxygen molecules on the backchannel region. Furthermore, IGZO TFT with MHO passivation exhibited superior PBS stability compared to conventional passivation layers (SiO<sub>2</sub> and HfO<sub>x</sub>), as shown in Figure S2.

When testing stability under light illumination (the NBIS test),  $V_{\rm TH}$  of IGZO TFTs shifted considerably for the unpassivated and monolayer-passivated (parylene-C, SiO<sub>2</sub>, and HfO<sub>x</sub>) IGZO TFTs, but the shift was negligible for the

MHO-passivated device as shown in Figures 2g and S3. Such a shift in  $V_{\rm TH}$  under light is attributable to ionization of uncoordinated oxygen species, which delivers extra electrons to the IGZO film. The small  $V_{\rm TH}$  shift of MHO-passivated IGZO TFTs indicates that the DPP-polymer film protects the IGZO film from illumination stress by absorbing light from above, whereas the parylene-C, SiO<sub>2</sub>, and HfO<sub>x</sub> layers, which are optically transparent, do not prevent irradiation from reaching the IGZO film. Therefore,  $V_{\rm TH}$  shift under the NBIS test is nearly identical to the NBS test for MHO-passivated devices.

To explore the role of layers in MHO passivation, we performed morphological, optical, and chemical analyses. Figure 3a,b compares the surface morphologies for IGZO, parylene-C/IGZO, and MHO/IGZO and contact angles for IGZO, parylene-C, and DPP-polymer films. From results of AFM images (Figure 3a), we observed that the surface roughness was little changed even after parylene-C coating on the IGZO film. Notably, when DPP-polymer was coated onto a parylene-C/IGZO film, the surface of the top layer became smoother. From contact angle measurements (Figure 3b), we found that parylene-C and DPP-polymer films showed a highly hydrophobic surface, whereas the IGZO film showed a somewhat-hydrophilic surface. This result indicates that parylene-C and DPP-polymer films effectively prevent charge modulation from adsorbing molecules by reducing the reactivity of the surface area of IGZO due to their hydrophobicity.<sup>29</sup> The hysteresis measurements (Figure 3c) revealed no change in the  $V_{\mathrm{TH}}$  after addition of the parylene-C and MHO layers, indicating that the interface between the IGZO and passivation layers was almost free of interface traps and defect sites. Further, we measured the transfer characteristics of IGZO TFTs with MHO passivation after soaking in water for 120 min as shown in Figure 3d to investigate their stability under severe conditions. Interestingly, they showed similar transfer characteristics before and after water soaking,

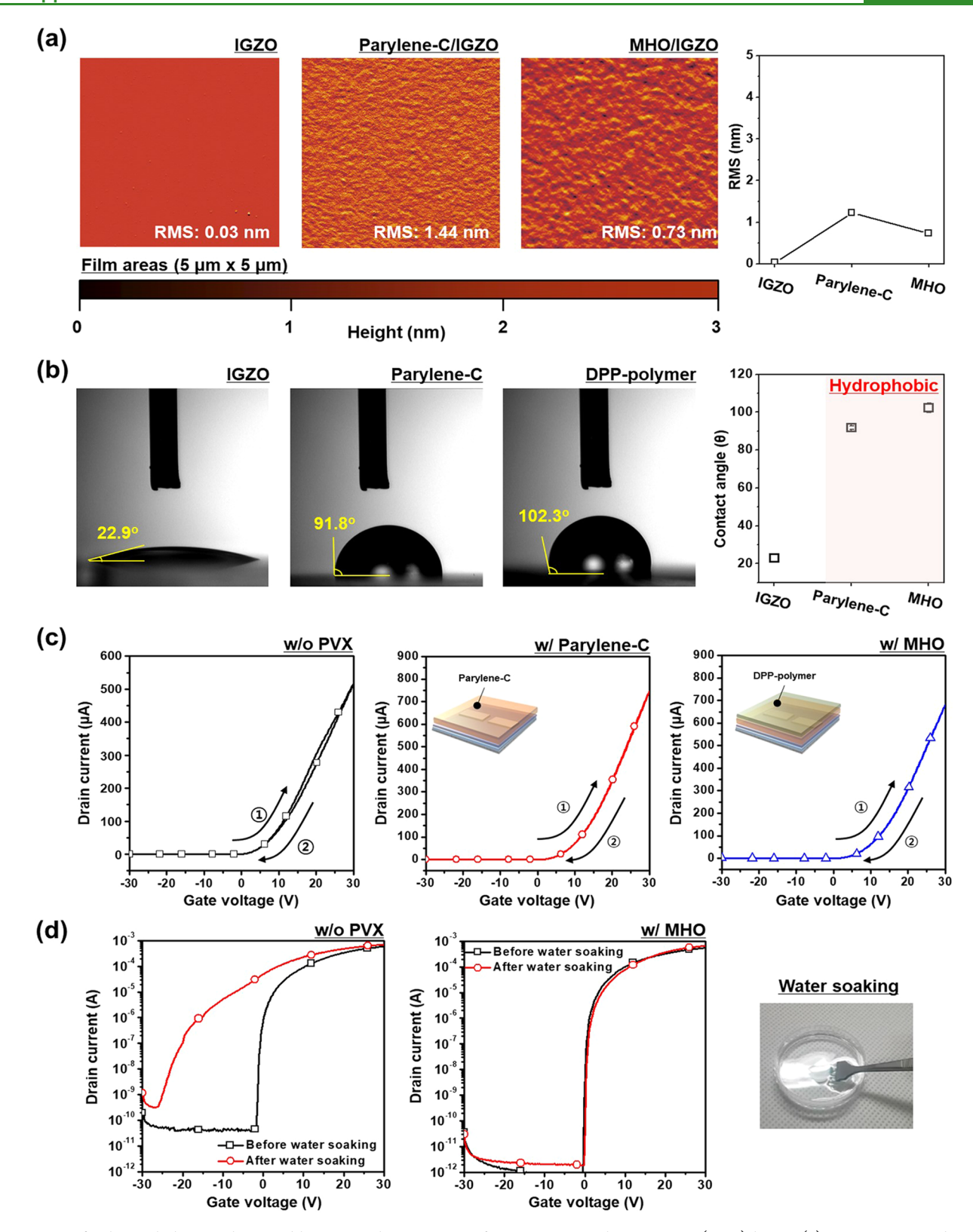


Figure 3. Surficial morphology analyses and hysteresis characteristics of IGZO TFTs with passivation (PVX) layers. (a) AFM images and surface roughness of the top layer: IGZO, parylene-C/IGZO, and MHO/IGZO films. (b) Contact angle analyses of IGZO, parylene-C, and DPP-polymer. (c) Hysteresis characteristics of IGZO TFTs, and (d) transfer characteristics of IGZO TFTs without passivation and with an MHO passivation layer upon water soaking for 120 min.

whereas the IGZO TFT without passivation exhibited severe degradation in its transfer characteristics after water soaking. This result demonstrates the excellent ability of the passivation layers to block moisture from the IGZO channel surface.

Figure 4 shows optical analyses to demonstrate how MHO passivation can significantly improve the stability of IGZO TFT under light illumination. Figure 4a compares the light absorbance at visible wavelengths by IGZO, parylene-C, and

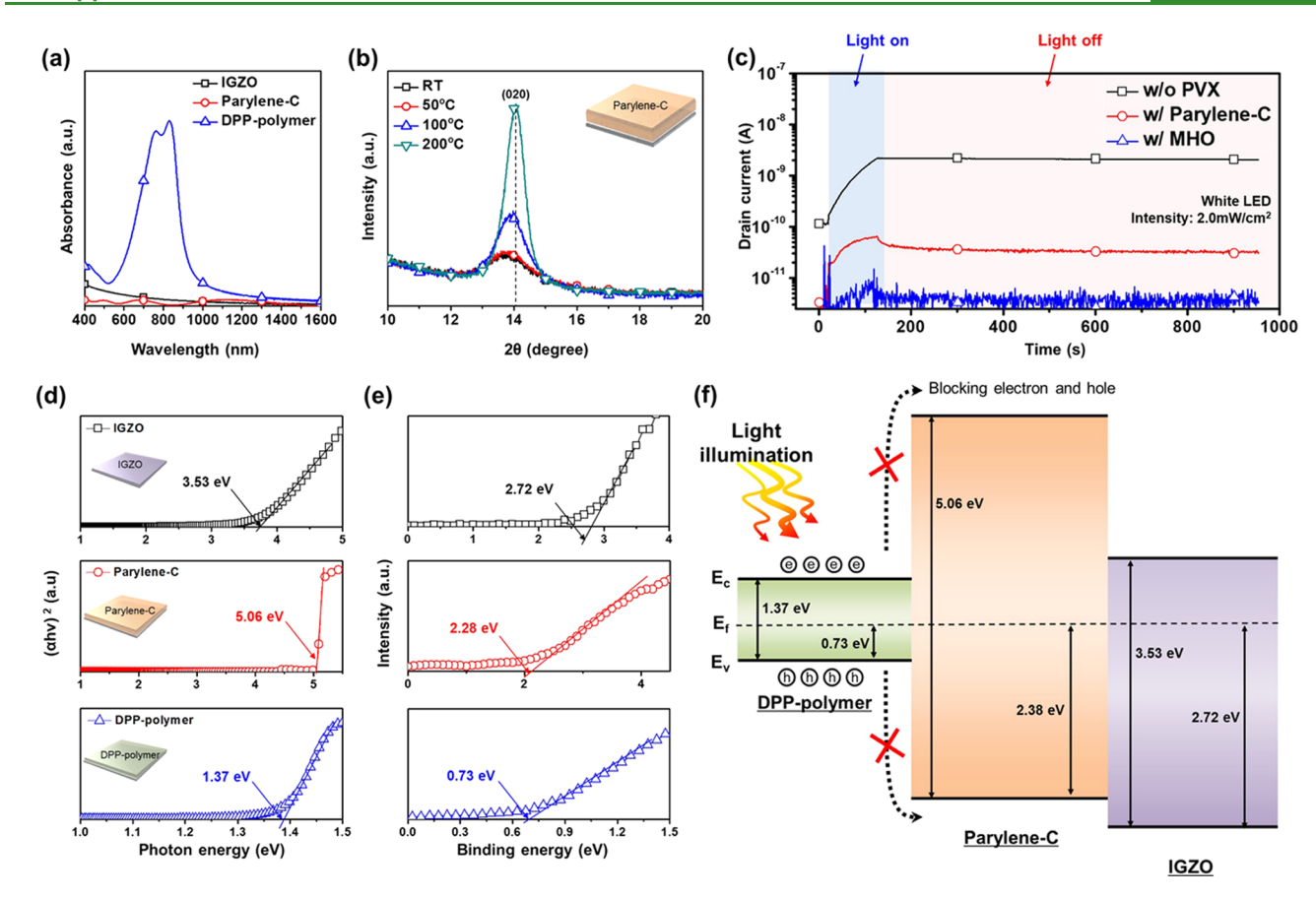


Figure 4. Optical analysis and design of band structure for the MHO passivation (PVX) layer. (a) Comparison of absorbance as a function of wavelength for IGZO, parylene-C, and DPP-polymer films. (b) XRD analysis of parylene-C with processing temperatures. (c) Change of drain current for IGZO TFTs without the passivation layer and with parylene-C and MHO passivation layers under white LED light illumination. Comparison of (d) optical band gaps and (e) valence band offset energies for IGZO, parylene-C, and DPP-polymer films. (f) Schematic of the band structure for IGZO TFTs with MHO passivation.

DPP-polymer films. The DPP-polymer film readily absorbed light in the visible to near-infrared region, while the parylene-C and IGZO films absorbed light poorly over the whole region, although absorption increased at shorter wavelengths. These results of light absorbance for IGZO, parylene-C, and DPPpolymer films were used to derive the optical band-gap energies of each film as shown in Figure 4d. The optical band gaps of IGZO, parylene-C, and DPP-polymer films were 3.53, 5.06, and 1.37 eV, respectively, based on Tauc's model. However, for the DPP-polymer film, its light absorbance lowered with decreased thickness (i.e., increased spin-coating speed) and increased processing temperature (Figure S4) because of a partial phase transformation from amorphous to semicrystalline, which has been demonstrated in previous reports.<sup>30</sup> Furthermore, on monitoring the X-ray diffraction (XRD) peak corresponding to the (020) crystal orientation of parylene-C films prepared at temperatures ranging from room temperature to 200 °C (Figure 4b), we found that the microstructure of parylene-C films was strongly influenced by processing temperature; an elevated processing temperature results in an increase in crystallinity.<sup>31</sup> Therefore, for MHO passivation, we intentionally fabricated DPP-polymer and parylene-C films at room temperature to achieve high light absorbance and ensure an amorphous microstructure, respectively. We optimized light absorption by the DPPpolymer film and reduced the carrier leakage current of the parylene-C film by eliminating grain boundaries. Figure 4f illustrates the band alignment of an IGZO film with the MHO passivation layer, based on the optical band-gap energy (Figure 4d) and valence band energy determined by XPS analysis in Figure 4e. The band alignments assume that the system is at equilibrium state. From the band alignments, we confirmed that most light can be absorbed by the DPP-polymer film because of its low optical band gap, while the parylene-C film prevents excitons generated within the DPP-polymer film from transferring to the IGZO channel because of the high conduction/valence offset between the DPP-polymer and parylene-C. In other words, by controlling the band structure and exploiting the intrinsic properties of the two layers, our MHO passivation prevents incident illumination stress on IGZO and then significantly improves the stability of IGZO TFTs under light illumination. However, as the DPP-polymer could not fully absorb the light, some light may reach the IGZO film. This energy can generate photoexcited carriers in the channel, which lead to a slight increase in drain current when illumination stress exists.

We also measured the variations in the drain current under prolonged light illumination time to investigate the persistence photocurrent (PPC) of IGZO TFTs with and without parylene-C and MHO passivation as shown in Figure 4c. We measured the drain current at a constant gate voltage ( $V_{\rm GS}$ ) and drain voltage ( $V_{\rm DS}$ ) of -1 and 10.1 V, respectively, under white LED light illumination (5700 lx). The drain current of IGZO TFT with MHO passivation barely changed under light

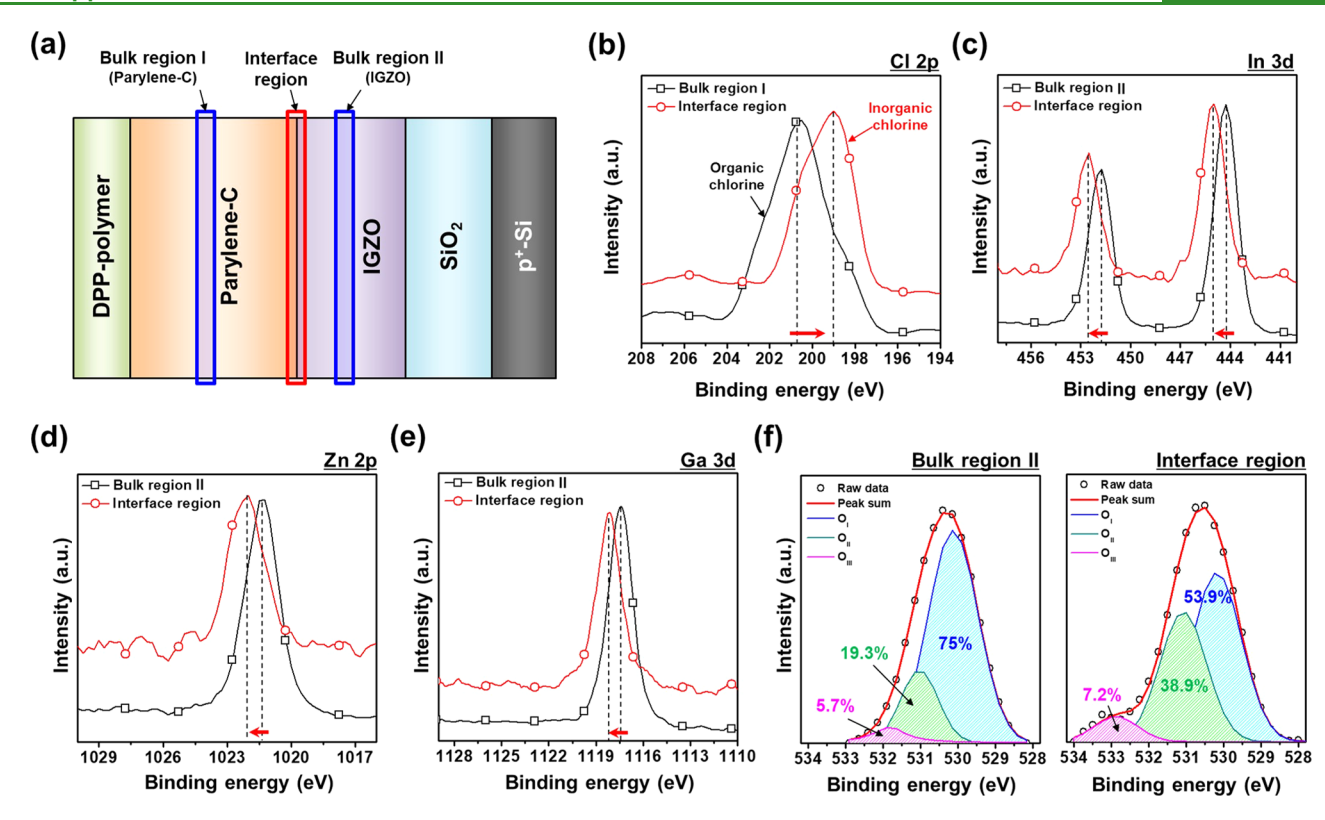


Figure 5. XPS analyses of bulk and interface regions in IGZO TFTs with the MHO passivation layer. (a) Schematic of various regions of XPS measurement in the MHO passivation layer. Comparison of the (b) chlorine 2p spectrum, (c) indium 3d spectrum, (d) zinc 2p spectrum, (e) gallium 3d spectrum, and (f) oxygen 1s spectrum in bulk and interface regions.

illumination, but the drain current of an IGZO TFT with only a parylene-C passivation layer increased significantly. Additionally, the increase in drain current remained in parylene-C passivated IGZO TFTs even after turning off the light. Furthermore, for the nonpassivated IGZO TFT, the drain current increased markedly under light illumination and did not decrease after turning off the light. This increase in drain current means that incident light was directly absorbed by the IGZO film-generated excitons and ionized uncoordinated oxygen species, triggering a severe PPC effect. To further investigate the light response of IGZO TFTs, we also measured a variation of drain currents under red, green, and blue laser illumination with different power intensities as shown in Figure S5. The wavelengths of the red, green, and blue lasers are 635, 532, and 405 nm, respectively. In the case of IGZO TFTs without passivation and with parylene-C passivation, the drain current increased sharply under green and blue laser illumination and further increased with increasing power intensity; however, the drain current was not affected by red laser illumination. This indicates that IGZO films contain high levels of uncoordinated oxygen species of ionization energy of about 2-3 eV so that they can be ionized sufficiently by green (2.33 eV) and blue (3.06 eV) but not red (1.95 eV) light. However, IGZO TFTs with MHO passivation showed a high stability under red, green, and blue laser light illumination, and the increase in drain current was negligible with increased power intensity. This is attributed to the high absorbance of the DPP-polymer layer in the visible light region and the additional effect of blocking photogenerated carriers due to the high conduction/valence offset between DPPpolymer and parylene-C layers.

Figure 5 presents depth XPS analyses of IGZO films with MHO passivation layers to examine the chemical compositions of each layer. We performed in situ XPS depth analysis to follow the chemical compositions of the bulk parylene-C layer (bulk region I), followed by the interface between parylene-C and IGZO (the interface region), followed by the bulk IGZO layer (bulk region II) as shown in Figure 5a. By performing in situ XPS depth measurements, we were able to confirm in real time where each layer began and ended. We could distinguish the distribution of the parylene-C layer and the interface between DPP-polymer and parylene-C from etched-out Cl elements because only parylene-C has the Cl elements among the layers of the device. Additionally, we could distinguish the distribution of the IGZO layer and interface between parylene-C and IGZO from etched-out In elements because In elements only exist at the IGZO layer in the whole device. Figure 5b shows the Cl 2p core-spectra of bulk region I and the interface region. It indicates that Cl atoms in bulk parylene-C and Cl atoms at the interface region were bonded differently in organic and inorganic formation networks, respectively, and those Cl atoms originating from different bonds demonstrated that the bonding between metal and Cl atoms was newly formed at the interface between parylene-C and IGZO. We observed a shift in the Cl 2p peak of the interface region to lower binding energies compared to the Cl 2p peak of bulk region I, confirming that Cl atoms accept electrons from the IGZO surface. Further, as the Cl 2p spectra are located at 201  $\pm$  0.2 and 199  $\pm$  0.3 eV in bulk region I and the interface region, respectively, the electron-accepting properties of Cl atoms in parylene-C enhance the electrical characteristics of the IGZO TFT. Cl atoms in oxide systems are widely accepted to passivate uncoordinated oxygen species because the Cl

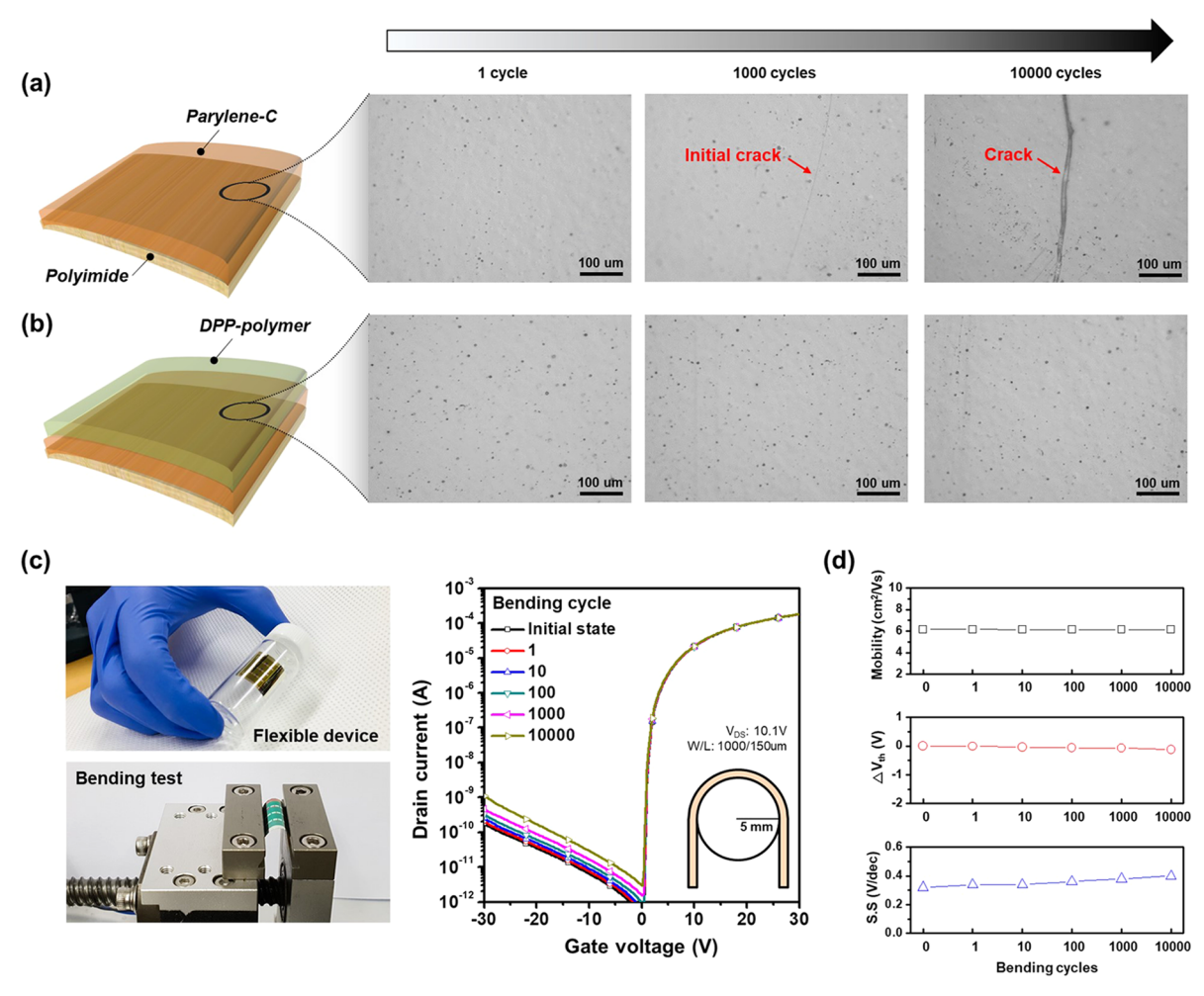


Figure 6. Mechanical test of MHO films and IGZO TFTs with MHO passivation. Top-view optical microscopy image of (a) parylene-C and (b) MHO films on polyimide substrate. (c) Photo of flexible IGZO TFTs with MHO passivation and bending test, and transfer characteristics with bending cycles at 5 mm curvature radius. (d) Variation of electrical parameters with bending cycles.

atomic radius is similar to that of an oxygen ion, but the standard electrode potential of the Cl atom is higher than those of In and Zn. 32,33 Furthermore, we observed a negligible change in the binding energy of the carbon 1s peak of the carbon species in parylene-C during the XPS depth analysis as shown in Figure S6. To investigate the decrease in uncoordinated oxygen species, we measured the XPS corespectra of In, Zn, Ga, and O at the interface and in bulk region II, shown in Figure 5c-f, respectively. In Figure 5f, O<sub>1</sub>, O<sub>1</sub>, and O<sub>III</sub> denote the relative metal-oxide (M-O) bonds, uncoordinated oxygen species, and hydroxyl groups (M-OH), respectively. The relative amounts of these species are quantified in Figure 5f. Our results show that In, Zn, and Ga metal peaks in the interface region were shifted to higher binding energies with no change in the spectral shape compared to those of bulk region II. These metal cations in the interface region have a higher oxidation state than those in bulk region II, indicating a stronger ionic bond between the metal cation and oxygen anion or Cl species from parylene-C. Indeed, bonding energies of In-Cl (439 kJ/mol), Zn-Cl (229 kJ/mol), and Ga-Cl (481 kJ/mol) were higher than those of In-O (360 kJ/mol), Zn-O (284 kJ/mol), and Ga-O (285 kJ/ mol).34-36

Finally, we verified the flexibility of MHO films and IGZO TFTs with MHO passivation using a mechanical bending test

as shown in Figure 6. Figure 6a,b shows optical microscopic images as a function of the bending cycle number for parylene-C and MHO films coated onto polyimide, respectively. These figures show a top-view image for each film after it was stressed for 1, 1000, and 10 000 cycles at a radius of curvature of 5 mm. After 10 000 cycles, a line crack was observed in the parylene-C film, but the MHO film showed no signs of crack. The robust properties of the MHO film suggest that addition of the DPPpolymer film improves the flexibility of the parylene-C film. The compressive/tensile stress applied to the parylene-C layer during bending stress seems to be compensated by stacking DPP-polymer. Figure S7 shows optical microscopy images of only polyimide films up to 10 000 bending cycles, which indicate polyimide films were not deformed during the bending test. We also measured the transfer characteristics of flexible IGZO TFTs with MHO passivation as a function of bending cycles, shown in Figure 6c. Interestingly, although the offcurrent is slightly increased with the bending cycle number, the transfer characteristics were barely changed; there were little variations in the electrical properties such as field-effect mobility,  $V_{\text{TH}}$  shift, and S.S with bending cycles (Figure 6d). Thus, these results showed that most mechanical stress is concentrated on the outermost MHO passivation layer, rendering the IGZO channel layer insensitive to repetitive mechanical stresses.

#### 4. CONCLUSIONS

In this work, we presented an MHO passivation layer formed at room temperature by sequentially stacking parylene-C and DPP-polymer films onto the back-channel of the IGZO film. While conventional passivation layers are intended to block adsorbed molecules, our proposed MHO passivation performs several functions, which enhance the performance of IGZO TFTs through an exclusive heterogeneous band structure and each film's intrinsic properties: (1) improvement of IGZO TFT's electrical characteristics by forming chemical bonds with Cl in the back-channel region, (2) prevention of interactions with adsorbed molecules on the back-channel region due to its hydrophobicity, and (3) blocking light absorption into the IGZO films directly by steplike band alignment. Furthermore, IGZO TFTs with an MHO passivation layer exhibited considerable reliability under harsh conditions such as soaking in water for 120 min and visible light illumination. Finally, the MHO film's flexibility was significantly improved so that flexible IGZO TFTs with an MHO passivation layer showed high mechanical stability over 10 000 cycles at 5 mm curvature radius.

## ASSOCIATED CONTENT

# **S** Supporting Information

The Supporting Information is available free of charge at https://pubs.acs.org/doi/10.1021/acsami.9b16898.

Chemical structure of materials for the MHO passivation layer; PBS and NBIS stabilities of IGZO TFTs with passivation layers; comparison of absorbance property as a function of spin-coating speed and process temperature for DPP-polymer; change of drain current for IGZO TFTs with passivation layers as a function of red, green, and blue laser power; XPS analysis of the carbon 1s spectrum in bulk and interface regions in IGZO TFTs with the MHO passivation layer; optical microscopy for the mechanical test of the polyimide substrate (PDF)

## AUTHOR INFORMATION

## **Corresponding Authors**

\*E-mail: asalleo@stanford.edu (A.S.). \*E-mail: hjk3@yonsei.ac.kr (H.J.K.).

ORCID

Scott Tom Keene: 0000-0002-6635-670X Si Joon Kim: 0000-0001-9191-9079 Hyun Jae Kim: 0000-0002-6879-9256

**Notes** 

The authors declare no competing financial interest.

## ACKNOWLEDGMENTS

This work was supported by the National Research Foundation of Korea (NRF) Grant funded by the Korea government (MSIP) (No. 2017R1A2B3008719). Part of this work was performed at the Stanford Nano Shared Facilities (SNSF) supported by the National Science Foundation (NSF) under award ECCS-1542152. S.T.K. and A.S. acknowledge financial support from the National Science Foundation (NSF) and Semiconductor Research Corporation (SRC), Award #1739795. Additionally, S.T.K. acknowledges the Stanford Office of Technology Licensing Stanford Graduate Fellowship fund (KAWBR-6037395) for support.

## REFERENCES

- (1) Nomura, K.; Ohta, H.; Takagi, A.; Kamiya, T.; Hirano, M.; Hosono, H. Room-temperature fabrication of transparent flexible thin-film transistors using amorphous oxide semiconductors. *Nature* **2004**, 432, 488–492.
- (2) Street, R. A. Thin-film transistors. Adv. Mater. 2009, 21, 2007—2022.
- (3) Ahn, B. D.; Shin, H. S.; Kim, G. H.; Park, J.-S.; Kim, H. J. A Novel Amorphous InGaZnO Thin Film Transistor Structure without Source/Drain Layer Deposition. *Jpn. J. Appl. Phys.* **2009**, *48*, No. 03B019.
- (4) Fortunato, E.; Barquinha, P.; Martins, R. Oxide semiconductor thin-film transistors: a review of recent advances. *Adv. Mater.* **2012**, 24, 2945–2986.
- (5) Kim, W.-G.; Tak, Y. J.; Kim, H. J. Nitrocellulose-based collodion gate insulator for amorphous indium zinc gallium oxide thin-film transistors. *J. Inf. Disp.* **2018**, *19*, 39–43.
- (6) Kamiya, T.; Hosono, H. Material characteristics and applications of transparent amorphous oxide semiconductors. *NPG Asia Mater.* **2010**, *2*, 15–22.
- (7) Wager, J. F. Oxide TFTs: A progress report. J. Inf. Disp. 2016, 32, 16-21.
- (8) Grimaud, A.; Diaz-Morales, O.; Han, B.; Hong, W. T.; Lee, Y.-L.; Giordano, L.; Stoerzinger, K. A.; Koper, M. T.; Shao-Horn, Y. Activating lattice oxygen redox reactions in metal oxides to catalyse oxygen evolution. *Nat. Chem.* **2017**, *9*, 457–465.
- (9) Wei, C.; Feng, Z.; Scherer, G. G.; Barber, J.; Shao-Horn, Y.; Xu, Z. Cations in Octahedral Sites: A Descriptor for Oxygen Electrocatalysis on Transition-Metal Spinels. *Adv. Mater.* **2017**, 29, No. 1606800.
- (10) Gosain, D. P.; Tanaka, T. Instability of amorphous indium gallium zinc oxide thin film transistors under light illumination. *Jpn. J. Appl. Phys.* **2009**, *48*, No. 03B018.
- (11) Ryu, B.; Noh, H.-K.; Choi, E.-A.; Chang, K.-J. O-vacancy as the origin of negative bias illumination stress instability in amorphous In—Ga—Zn—O thin film transistors. *Appl. Phys. Lett.* **2010**, 97, No. 022108.
- (12) Chowdhury, M. D. H.; Migliorato, P.; Jang, J. Light induced instabilities in amorphous indium—gallium—zinc—oxide thin-film transistors. *Appl. Phys. Lett.* **2010**, *97*, No. 173506.
- (13) Li, Y.; Lan, L.; Sun, S.; Lin, Z.; Gao, P.; Song, W.; Song, E.; Zhang, P.; Peng, J. All inkjet-printed metal-oxide thin-film transistor array with good stability and uniformity using surface-energy patterns. *ACS Appl. Mater. Interfaces* **2017**, *9*, 8194–8200.
- (14) Kwon, J. M.; Jung, J.; Rim, Y. S.; Kim, D. L.; Kim, H. J. Improvement in negative bias stress stability of solution-processed amorphous In–Ga–Zn–O thin-film transistors using hydrogen peroxide. ACS Appl. Mater. Interfaces 2014, 6, 3371–3377.
- (15) Chowdhury, M. D. H.; Mativenga, M.; Um, J. G.; Mruthyunjaya, R. K.; Heiler, G. N.; Tredwell, T. J.; Jang, J. Effect of  ${\rm SiO_2}$  and  ${\rm SiO_2/SiN_x}$  passivation on the stability of amorphous indium-gallium zinc-oxide thin-film transistors under high humidity. *IEEE Trans. Electron Devices* **2015**, *62*, 869–874.
- (16) Olziersky, A.; Barquinha, P.; Vilà, A.; Pereira, L.; Gonçalves, G.; Fortunato, E.; Martins, R.; Morante, J. R. Insight on the SU-8 resist as passivation layer for transparent Ga<sub>2</sub>O<sub>3</sub>–In<sub>2</sub>O<sub>3</sub>–ZnO thin-film transistors. *J. Appl. Phys.* **2010**, *108*, No. 064505.
- (17) Dong, C.; Shi, J.; Wu, J.; Chen, Y.; Zhou, D.; Hu, Z.; Xie, H.; Zhan, R.; Zou, Z. Improvements in passivation effect of amorphous InGaZnO thin film transistors. *Mater. Sci. Semicond. Process.* **2014**, 20, 7–11.
- (18) Bermundo, J. P.; Ishikawa, Y.; Yamazaki, H.; Nonaka, T.; Uraoka, Y. Highly reliable polysilsesquioxane passivation layer for a-InGaZnO thin-film transistors. *ECS J. Solid State Sci. Technol.* **2014**, 3, Q16–Q19.
- (19) Shin, K. Y.; Tak, Y. J.; Kim, W.-G.; Hong, S.; Kim, H. J. Improvement of electrical characteristics and stability of amorphous indium gallium zinc oxide thin film transistors using nitrocellulose passivation layer. *ACS Appl. Mater. Interfaces* **2017**, *9*, 13278–13285.

- (20) Hong, S.; Park, S. P.; Kim, Y.-g.; Kang, B. H.; Na, J. W.; Kim, H. J. Low-temperature fabrication of an HfO<sub>2</sub> passivation layer for amorphous indium—gallium—zinc oxide thin film transistors using a solution process. *Sci. Rep.* **2017**, *7*, No. 16265.
- (21) Kwon, G.; Kim, K.; Choi, B. D.; Roh, J.; Lee, C.; Noh, Y. Y.; Seo, S.; Kim, M. G.; Kim, C. Multifunctional Organic-Semiconductor Interfacial Layers for Solution-Processed Oxide-Semiconductor Thin-Film Transistor. *Adv. Mater.* **2017**, *29*, No. 1607055.
- (22) Karpov, Y.; Erdmann, T.; Raguzin, I.; Al-Hussein, M.; Binner, M.; Lappan, U.; Stamm, M.; Gerasimov, K. L.; Beryozkina, T.; Bakulev, V. High Conductivity in Molecularly p-Doped Diketopyrrolopyrrole-Based Polymer: The Impact of a High Dopant Strength and Good Structural Order. *Adv. Mater.* 2016, 28, 6003–6010.
- (23) Di Pietro, R.; Erdmann, T.; Carpenter, J. H.; Wang, N.; Shivhare, R. R.; Formanek, P.; Heintze, C.; Voit, B.; Neher, D.; Ade, H. Synthesis of High-Crystallinity DPP Polymers with Balanced Electron and Hole Mobility. *Chem. Mater.* **2017**, *29*, 10220–10232.
- (24) Bae, C.; Kim, D.; Moon, S.; Choi, T.; Kim, Y.; Kim, B. S.; Lee, J.-S.; Shin, H.; Moon, J. Aging dynamics of solution-processed amorphous oxide semiconductor field effect transistors. *ACS Appl. Mater. Interfaces* **2010**, *2*, 626–632.
- (25) Shin, J. H.; Lee, J. S.; Hwang, C. S.; Park, S. H. K.; Cheong, W. S.; Ryu, M.; Byun, C. W.; Lee, J. I.; Chu, H. Y. Light effects on the bias stability of transparent ZnO thin film transistors. *Etri J.* **2009**, *31*, 62–64.
- (26) Jang, H.-J.; Gu, J.-G.; Cho, W.-J. Sensitivity enhancement of amorphous InGaZnO thin film transistor based extended gate field-effect transistors with dual-gate operation. *Sens. Actuators, B* **2013**, 181, 880–884.
- (27) Jeong, J. K.; Won Yang, H.; Jeong, J. H.; Mo, Y.-G.; Kim, H. D. Origin of threshold voltage instability in indium-gallium-zinc oxide thin film transistors. *Appl. Phys. Lett.* **2008**, 93, No. 123508.
- (28) Jeon, S.; Ahn, S.-E.; Song, I.; Kim, C. J.; Chung, U.-I.; Lee, E.; Yoo, I.; Nathan, A.; Lee, S.; Ghaffarzadeh, K.; Robertson, J.; Kim, K. Gated three-terminal device architecture to eliminate persistent photoconductivity in oxide semiconductor photosensor arrays. *Nat. Mater.* **2012**, *11*, 301–305.
- (29) Choi, S.; Jo, J.-W.; Kim, J.; Song, S.; Kim, J.; Park, S. K.; Kim, Y.-H. Static and Dynamic Water Motion-Induced Instability in Oxide Thin-Film Transistors and Its Suppression by Using Low-k Fluoropolymer Passivation. ACS Appl. Mater. Interfaces 2017, 9, 26161–26168.
- (30) Ma, T.; Jiang, K.; Chen, S.; Hu, H.; Lin, H.; Li, Z.; Zhao, J.; Liu, Y.; Chang, Y.; Hsiao, C. Efficient Low-Bandgap Polymer Solar Cells with High Open-Circuit Voltage and Good Stability. *Adv. Energy Mater.* **2015**, *5*, No. 1501282.
- (31) Kim, H. T.; Kim, C. D.; Lee, S. Y.; Sohn, Y. S. Effects of annealing temperature on Parylene-C films formed by chemical vapor condensation method. *Mol. Cryst. Liq. Cryst.* **2015**, *618*, 139–145.
- (32) Rousset, J.; Saucedo, E.; Lincot, D. Extrinsic doping of electrodeposited zinc oxide films by chlorine for transparent conductive oxide applications. *Chem. Mater.* **2009**, 21, 534–540.
- (33) Lupan, O.; Pauporté, T.; Chow, L.; Viana, B.; Pellé, F.; Ono, L.; Cuenya, B. R.; Heinrich, H. Effects of annealing on properties of ZnO thin films prepared by electrochemical deposition in chloride medium. *Appl. Surf. Sci.* **2010**, 256, 1895–1907.
- (34) Kim, C.; Efremov, A.; Lee, J.; Han, I. K.; Kim, Y.-H.; Kwon, K.-H. Kinetics and mechanisms for ion-assisted etching of InP thin films in HBr + Cl<sub>2</sub> + Ar inductively coupled plasma with various HBr/Cl<sub>2</sub> mixing ratios. *Thin Solid Films* **2018**, *660*, 590–595.
- (35) Woo, J.-C.; Um, D.-S.; Kim, C.-I. The dry etching of a sol-gel deposited ZnO thin film in a high density BCl<sub>3</sub>/Ar plasma. *Thin Solid Films* **2010**, *518*, 2905–2909.
- (36) Lu, Z. Xanes studies of III-V semiconductor surface passivation. *Prog. Surf. Sci.* **1995**, *50*, 335–345.